High frequency homogenization for periodic media

By R. V. Craster[1], J. Kaplunov[2] & A. V. Pichugin[2]

[1] *Department of Mathematical and Statistical Sciences, University of Alberta, Edmonton, T6G 2G1, Canada*

[2] *Department of Mathematical Sciences, Brunel University, Uxbridge, Middlesex, UB8 3PH, U.K.*

1 December 2014

An asymptotic procedure based upon a two-scale approach is developed for wave propagation in a doubly periodic inhomogeneous medium with a characteristic lengthscale of microstructure far less than that of the macrostructure. In periodic media there are frequencies for which standing waves, periodic with the period or double-period of the cell, on the microscale emerge. These frequencies do not belong to the low frequency range of validity covered by classical homogenization theory, which motivates our use of the term "high frequency homogenization" when perturbing about these standing waves. The resulting long wave equations are deduced only explicitly dependent upon the macroscale, with the microscale represented by integral quantities. These equations accurately reproduce the behaviour of the Bloch mode spectrum near the edges of the Brillouin zone, hence yielding an explicit way for homogenizing periodic media in the vicinity of "cell resonances". The similarity of such model equations to high frequency long wavelength asymptotics, for homogeneous acoustic and elastic waveguides, valid in the vicinities of thickness resonances is emphasized. Several illustrative examples are considered and show the efficacy of the developed techniques.

Keywords: Floquet-Bloch waves; Stop bands; Photonics; Phononics; High frequency long waves; homogenization

1. Introduction

Many structures are constructed from composites with periodic, or doubly-periodic, variations in material parameters. The varied, and sometimes unexpected wave propagation properties of composites (Milton, 2002) have motivated a number of remarkable new applications, including, but not limited to, photonic crystals and microstructured fibres (Joannopoulos *et al.*, 1995; Zolla *et al.*, 2005), as well as the rapidly developing area of metamaterials (Smith *et al.*, 2004). Thus, there is considerable interest in modelling wave propagation through media with regularly spaced defects or inhomogeneities. Direct numerical simulation using finite elements (Zolla *et al.*, 2005) is popular, but can become intensive for large scale media with many small inclusions even if calculated over a single cell with Floquet-Bloch conditions invoked. In the latter case progress can also be made using Rayleigh's multipole method (Rayleigh, 1892) and modern extensions and refinements are possible

(Movchan *et al.*, 2002; Poulton *et al.*, 2009). Another popular procedure is the plane wave expansion method that amounts to expanding all relevant fields over the cell into Fourier series and solving the resulting infinite system of linear equations (Kushwaha *et al.*, 1993; Andrianov *et al.*, 2008).

Complementary to this literature is that of homogenization, which involves taking a medium with rapidly oscillatory material properties on a fine microscale and averaging these out, in some fashion, to obtain an equivalent homogeneous material with effective material parameters. This is naturally convenient as it buries the microstructure into coefficients, and computations, or analysis, are then just performed on the macroscale. The development of traditional techniques of asymptotic homogenization has been strongly focused on recovering the classical limiting behaviours in effective media (Sanchez-Palencia, 1980; Bakhvalov & Panasenko, 1989). This usually implies slow variation of relevant fields both on the microscale and macroscale, which limits the applicability of the associated expansions to low frequency situations, see e.g. Parnell & Abrahams (2006) or Andrianov *et al.* (2008). While the frequency range of such models can be extended by considering higher-order correction terms (Santosa & Symes, 1991; Bakhvalov & Eglit, 2000; Smyshlyaev & Cherednichenko, 2000), the resulting models cannot fully reproduce high frequency dynamic behaviours characteristic of microstructured materials, such as strong dispersion, the presence of band gaps or negative refraction. The other way to describe this limitation of the traditional homogenization theory would be to say that it is only capable of describing the fundamental Bloch mode at low frequencies. When inclusions are small with respect to the period, it is possible to construct "wide-spacing" approximation schemes capable of reproducing higher Bloch modes (Poulton *et al.*, 2001; McIver, 2007).

Traditional homogenization holds the frequency fixed while the natural small parameter tends to zero which is incompatible with the rapidly oscillating fields characteristic of higher Bloch modes. Bensoussan *et al.* (1978) demonstrate that in order to obtain the complete spectrum of Bloch modes, in their notation, one needs to scale frequency as the inverse of the natural small parameter, i.e., to consider the high frequency regime. Even at leading order, fields obtained in this asymptotic limit oscillate on the microscale, hence motivating the use of the WKB ansatz by Bensoussan *et al.* (1978). Intuitively, this may seem to contradict the very definition of what homogenization is usually thought to achieve. Nevertheless, for fields oscillating at the microscale, the variation of the solution from one periodicity cell to another can be very small. The high-frequency homogenization we develop is designed to exploit this situation and aims to model the *modulation* of the strongly oscillating field. Although very different from the physical point of view, a mathematically similar asymptotic regime is also observed in the so-called "double porosity limit" of high-contrast homogenization, see e.g. Arbogast *et al.* (1990). When contrast in material parameters is sufficiently large, higher Bloch modes may become part of the low frequency response; this has been recently studied in the context of wave propagation (Babych *et al.*, 2008; Smyshlyaev, 2009).

For periodic, and doubly-periodic, media the interest is often in identifying the Bloch spectra and stop band structure of the solution (Zolla *et al.*, 2005). The Bloch spectra at the edges of the irreducible Brillouin zone correspond to standing waves (Brillouin, 1953). Our aim is to develop a high frequency asymptotic procedure based upon perturbing about these standing wave solutions occurring at particular

frequencies across a periodic structure. Taking advantage of the scale separation between micro- and macroscales the standing waves can be considered upon the microscale and then "averaged" to get a problem just upon the macroscale. The existence of a differential operator of this type has been recently proved rigorously (Birman, 2004; Birman & Suslina, 2006). The upshot of our analysis is that an effective partial differential equation is constructed on the macroscale that is valid for frequencies in the vicinity of the standing wave. The coefficients of this equation involve integrals of the standing wave solutions and an auxiliary solution along an elementary cell on the microscale. The problem is therefore homogenized in the sense that the microscale plays no explicit role in the effective model. However, in contrast to classical homogenization, the asymptotic macroscale equation is strongly dispersive and can be used to model a range of dynamic phenomena characteristic for composite media. The final form of the effective model bears remarkable similarity to high frequency long wave equations in asymptotic theories, for elastic and acoustic waveguides, valid in the vicinity of thickness resonances (Berdichevski, 1983; Kaplunov *et al.*, 1998; Le, 1999; Gridin *et al.*, 2005).

The paper is structured as follows. In Section 2 we take a two-dimensional structure and develop an asymptotic procedure where we perturb away from standing wave solutions. The exposition of the two-dimensional case is simplified by considering standing waves with period of exactly one cell size. Very similar expansions can be constructed in the vicinity of standing waves with the period of two cell sizes along one or both coordinates; motivated by the form of corresponding boundary conditions we term such waves *anti-periodic*. The point is explicitly demonstrated for one-dimensional examples treated in Section 2(a). Illustrative examples aimed at showing the accuracy of the asymptotics for Floquet-Bloch problems are then chosen. A piecewise homogeneous medium, Section 3(a), illustrates the influence of double roots in the Bloch spectra. The piecewise homogeneous string on a Winkler foundation, Section 3(b), has a lowest curve in the spectra that does not pass through the origin, and a low frequency band gap, allowing us to contrast the asymptotics developed here with the classical theory. A string with periodically varying density considered in Section 3(c) leads us to a Mathieu equation for which the leading order solutions can have a degeneracy that must be overcome, and is a non-trivial example for which the asymptotics are pursued using numerical methods. Some concluding remarks are drawn together in Section 4.

2. General theory

For generality we consider a regular periodic structure composed of inclusions and a matrix material. The inclusions are defined on a short-scale, l, that of the microstructure, whereas the overall problem is considered on a macroscale L which can be thought of as a typical wavelength dominating the dynamic response, or an overall dimension of the structure. The ratio of these scales, $\varepsilon \equiv l/L$, is assumed small and provides a natural small parameter. The microstructure is characterized by functions $\hat{a}(x_1/l, x_2/l)$ and $\hat{\rho}(x_1/l, x_2/l)$ that are periodic in $\boldsymbol{\xi} = (x_1/l, x_2/l)$ and can be smooth functions, or piecewise continuous; $\mathbf{x} = (x_1, x_2)$ are Cartesian coordinates orientated along the edges of the cell.

We consider a model wave equation, for, say, SH waves in anti-plane elasticity with periodic density $\hat{\rho}(\boldsymbol{\xi})$ and shear modulus $\hat{a}(\boldsymbol{\xi})$, and with time harmonic

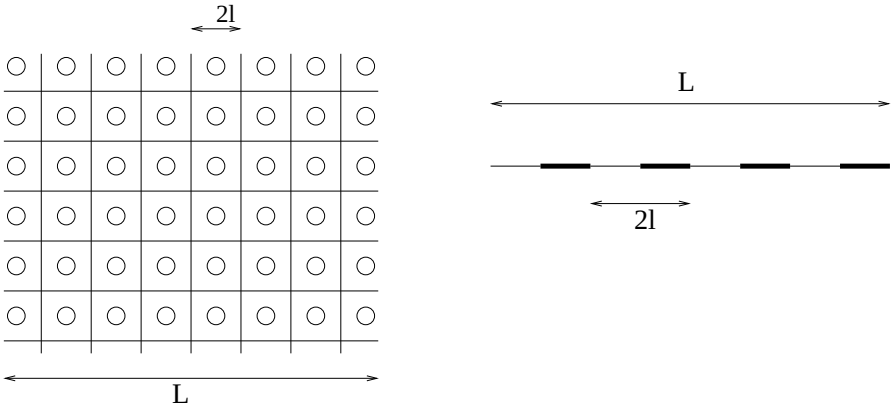

Figure 1. The geometry under consideration on the left showing a typical two-dimensional structure with microstructure of scale l and macrostructure on scale L. On the right, a one dimensional model structure, a piecewise homogeneous string, considered in Section 2(a).

dependence $\exp(-i\omega t)$ assumed understood, as

$$\nabla_{\mathbf{x}} \cdot [\hat{a}(\boldsymbol{\xi})\nabla_{\mathbf{x}} u(\mathbf{x})] + \omega^2 \hat{\rho}(\boldsymbol{\xi}) u(\mathbf{x}) = 0 \tag{2.1}$$

on $-\infty < x_1, x_2 < \infty$ with $\nabla_{\mathbf{x}}$ as the gradient operator with respect to the $\mathbf{x}$ coordinates. The material parameters in (2.1) can be measured in their typical unit values, so that $\hat{a} \equiv \hat{a}_0 a(\boldsymbol{\xi})$ and $\hat{\rho} \equiv \hat{\rho}_0 \rho(\boldsymbol{\xi})$, with the absence of hats indicating non-dimensionality. In this case (2.1) transforms to

$$l^2 \nabla_{\mathbf{x}} \cdot [a(\boldsymbol{\xi})\nabla_{\mathbf{x}} u(\mathbf{x})] + \lambda^2 \rho(\boldsymbol{\xi}) u(\mathbf{x}) = 0 \quad \text{with} \quad \lambda = \frac{\omega l}{\hat{c}_0} \tag{2.2}$$

with $\hat{c}_0 = \sqrt{\hat{a}_0/\hat{\rho}_0}$ a characteristic wave speed. We adopt a multiple scales approach treating the disparate lengthscales $\mathbf{X} = \mathbf{x}/L$, and $\boldsymbol{\xi} = \mathbf{x}/l$ as new independent variables with the result that (2.2) becomes

$$\begin{aligned} &\nabla_{\boldsymbol{\xi}} \cdot [a(\boldsymbol{\xi})\nabla_{\boldsymbol{\xi}} u(\mathbf{X}, \boldsymbol{\xi})] + \lambda^2 \rho(\boldsymbol{\xi}) u(\mathbf{X}, \boldsymbol{\xi}) \\ &\quad + \varepsilon [2a(\boldsymbol{\xi})\nabla_{\boldsymbol{\xi}} + \nabla_{\boldsymbol{\xi}} a(\boldsymbol{\xi})] \cdot \nabla_{\mathbf{X}} u(\mathbf{X}, \boldsymbol{\xi}) + \varepsilon^2 a(\boldsymbol{\xi}) \nabla^2_{\mathbf{X}} u(\mathbf{X}, \boldsymbol{\xi}) = 0 \end{aligned} \tag{2.3}$$

where the separation of scales is now made explicit. The notations $\nabla_{\boldsymbol{\xi}}$ and $\nabla_{\mathbf{X}}$ denote $(\partial_{\xi_1}, \partial_{\xi_2})$ and $(\partial_{X_1}, \partial_{X_2})$ respectively. Classical homogenization theory is usually concerned with $\lambda \ll 1$, see (2.2), the crucial distinction of high-frequency homogenization allows for $\lambda \sim O(1)$.

We develop the methodology for perturbations to standing wave solutions that are periodic on the cell. If we take the periodicity in $\boldsymbol{\xi}$ to be on a square cell with $-1 \le \xi_i \le 1$, for $i = 1, 2$ then periodicity conditions are to be taken in $\boldsymbol{\xi}$ along the edges of the cell namely:

$$u|_{\xi_1=1} = u|_{\xi_1=-1}, \qquad u|_{\xi_2=1} = u|_{\xi_2=-1}, \tag{2.4}$$

$$u_{\xi_1}|_{\xi_1=1} = u_{\xi_1}|_{\xi_1=-1}, \qquad u_{\xi_2}|_{\xi_2=1} = u_{\xi_2}|_{\xi_2=-1}. \tag{2.5}$$

The corresponding solution $u(\mathbf{X}, \boldsymbol{\xi})$ will be periodic in $\boldsymbol{\xi}$, but not necessarily in $\mathbf{X}$. One can replace these periodicity conditions along one or both spatial dimensions with special "out-of-phase" boundary conditions. These *anti-periodic* boundary conditions lead to solutions that are periodic across two cells in the appropriate direction(s) of $\boldsymbol{\xi}$. For the sake of clarity we specialize the two-dimensional derivations to the case periodic in both ξ_1 and ξ_2 for which (2.4,2.5) apply. We illustrate the application and consequences of anti-periodic boundary conditions only for the one-dimensional case presented in Section 2(a).

Next we adopt the ansatz:

$$u(\mathbf{X}, \boldsymbol{\xi}) = u_0(\mathbf{X}, \boldsymbol{\xi}) + \varepsilon u_1(\mathbf{X}, \boldsymbol{\xi}) + \varepsilon^2 u_2(\mathbf{X}, \boldsymbol{\xi}) + \ldots, \quad \lambda^2 = \lambda_0^2 + \varepsilon \lambda_1^2 + \varepsilon^2 \lambda_2^2 + \ldots \tag{2.6}$$

Each $u_i(\mathbf{X}, \boldsymbol{\xi})$ for $i = 1, 2 \ldots$, is periodic in $\boldsymbol{\xi}$, c.f. (2.4), (2.5). This ansatz assumes variation both at the microscale and macroscale even at leading order, as opposed to classical homogenization theory for which $u_0(\mathbf{X}, \boldsymbol{\xi}) \equiv u_0(\mathbf{X})$.

Substituting (2.6) into (2.3), and equating to zero the coefficients of individual powers of ε, we obtain a hierarchy of equations for $u_i(\mathbf{X}, \boldsymbol{\xi})$ and λ_i with associated boundary conditions from the periodicity in $\boldsymbol{\xi}$. This hierarchy is resolved from the lowest order up. At lowest order we obtain an eigenvalue problem for

$$\nabla_{\boldsymbol{\xi}} \cdot [a(\boldsymbol{\xi}) \nabla_{\boldsymbol{\xi}} u_0] + \lambda_0^2 \rho(\boldsymbol{\xi}) u_0 = 0 \tag{2.7}$$

subject to the appropriate periodicity boundary conditions. This gives rise to a discrete spectrum of eigenvalues λ_0^2 for which there is no phase shift across a period of the structure and standing wave is formed. If we fix a simple eigenvalue λ_0 then the corresponding eigenmode is of the form

$$u_0(\mathbf{X}, \boldsymbol{\xi}) = f_0(\mathbf{X}) U_0(\boldsymbol{\xi}, \lambda_0) \tag{2.8}$$

where $U_0(\boldsymbol{\xi}, \lambda_0)$ is a periodic function of $\boldsymbol{\xi}$ and $f_0(\mathbf{X})$ remains to be determined; we introduce λ_0 into the argument of the periodic function to emphasise that it depends upon the frequency λ_0. This leading order solution is exactly periodic on the cell hence conforming to the commonly used notion of the unit cell resonance (or micro-resonance). Notably, the case of coincident eigenvalues can also arise and is discussed in the simpler context for one-dimensional structures in the following section. Generally, the leading order problem would need to be solved numerically, as is the case in classical homogenization. Since we desire the corrections λ_1^2, λ_2^2 and the function $f_0(\mathbf{X})$ we continue with the hierarchy.

At next order the equation for $u_1(\mathbf{X}, \boldsymbol{\xi})$ is

$$\nabla_{\boldsymbol{\xi}} \cdot [a(\boldsymbol{\xi}) \nabla_{\boldsymbol{\xi}} u_1] + \lambda_0^2 \rho(\boldsymbol{\xi}) u_1 = -\nabla_{\mathbf{X}} f_0 \cdot [2a(\boldsymbol{\xi}) \nabla_{\boldsymbol{\xi}} U_0 + U_0 \nabla_{\boldsymbol{\xi}} a(\boldsymbol{\xi})] - f_0 \lambda_1^2 \rho(\boldsymbol{\xi}) U_0 \tag{2.9}$$

and we now invoke an orthogonality condition that involves multiplying (2.9) by U_0 and integrating over the periodic cell in $\boldsymbol{\xi}$. This yields

$$\begin{aligned} &\iint_S \left(U_0 \nabla_{\boldsymbol{\xi}} \cdot [a(\boldsymbol{\xi}) \nabla_{\boldsymbol{\xi}} u_1] + \lambda_0^2 \rho(\boldsymbol{\xi}) U_0 u_1 \right) dS \\ &\qquad = -\nabla_{\mathbf{X}} f_0 \cdot \iint_S \nabla_{\boldsymbol{\xi}} [a(\boldsymbol{\xi}) U_0^2] dS - f_0 \lambda_1^2 \iint_S \rho(\boldsymbol{\xi}) U_0^2 dS \end{aligned} \tag{2.10}$$

where $\iint_S$ denotes integration over the cell. Using a corollary to the divergence theorem, the first integral on the right hand side is converted to an integral along the edges of the cell, thereafter we use periodicity of $a(\boldsymbol{\xi})$ and U_0 and it vanishes. We now subtract the integral of (2.7), multiplied by u_1/f_0, over the cell, from (2.10), which results in

$$\iint_S (U_0 \nabla_{\boldsymbol{\xi}} \cdot [a(\boldsymbol{\xi}) \nabla_{\boldsymbol{\xi}} u_1] - u_1 \nabla_{\boldsymbol{\xi}} \cdot [a(\boldsymbol{\xi}) \nabla_{\boldsymbol{\xi}} U_0]) dS = -f_0 \lambda_1^2 \iint_S \rho(\boldsymbol{\xi}) U_0^2 dS. \quad (2.11)$$

Using Green's second identity the left-hand side becomes

$$\int_{\partial S} a(\boldsymbol{\xi}) \left(U_0 \frac{\partial u_1}{\partial n} - u_1 \frac{\partial U_0}{\partial n} \right) ds \quad (2.12)$$

where ∂S is the boundary of region S and n is the outward pointing normal. From periodicity in $\boldsymbol{\xi}$ of U_0, u_1 and a, this integral vanishes. Thus the only non-zero term is that multiplying λ_1^2, therefore λ_1 must be identically zero. An explicit solution for $u_1(\mathbf{X}, \boldsymbol{\xi})$, from (2.9), with $\boldsymbol{\xi}$ restricted to be in the cell S, is found as

$$u_1(\mathbf{X}, \boldsymbol{\xi}) = f_1(\mathbf{X}) U_0(\boldsymbol{\xi}, \lambda_0) + \nabla_{\mathbf{X}} f_0(\mathbf{X}) \cdot [\mathbf{V}_1(\boldsymbol{\xi}, \lambda_0) - \boldsymbol{\xi} U_0(\boldsymbol{\xi}, \lambda_0)], \quad (2.13)$$

where the coefficient, f_1, of the homogeneous solution does not appear, to leading order, in the final result and plays no further role here. The vector function $\mathbf{V}_1 = (V_1^{(1)}, V_1^{(2)})$ satisfies the leading order equation (2.7), that is,

$$\nabla_{\boldsymbol{\xi}} \cdot [a(\boldsymbol{\xi}) \nabla_{\boldsymbol{\xi}}] \mathbf{V}_1 + \lambda_0^2 \rho(\boldsymbol{\xi}) \mathbf{V}_1 = 0, \quad (2.14)$$

i.e. each component of $\mathbf{V}_1$ is the non-doubly periodic solution of (2.7) linearly independent of $U_0(\boldsymbol{\xi}, \lambda_0)$. Notably $u_1(\mathbf{X}, \boldsymbol{\xi})$ must be periodic in $\boldsymbol{\xi}$, however both terms in the square brackets of (2.13) are not. Therefore, we select each individual component of $\mathbf{V}_1$ to be periodic along one of the ξ_i and then choose its boundary conditions along the other ξ_j, $j \neq i$, in such a way that conditions (2.4)–(2.5) are enforced; the solution can then be periodically continued to the full structure. We set $V_1^{(1)}(\boldsymbol{\xi}, \lambda_0)$ to have periodicity in ξ_2 and then periodicity of u_1 in ξ_1 results in

$$V_1^{(1)}|_{\xi_1=1} - V_1^{(1)}|_{\xi_1=-1} = 2U_0|_{\xi_1=1} \quad (2.15)$$

$$V_{1\xi_1}^{(1)}|_{\xi_1=1} - V_{1\xi_1}^{(1)}|_{\xi_1=-1} = 2U_{0\xi_1}|_{\xi_1=1}. \quad (2.16)$$

Thus $V_1^{(1)}(\boldsymbol{\xi}, \lambda_0)$ is a periodic function in ξ_2 that must be found by solving the inhomogeneous boundary value problem given by equation (2.14) subject to boundary conditions consistent with (2.15) and (2.16), as well as $(2.4)_2$ and $(2.5)_2$.

Similarly we take $V_1^{(2)}(\boldsymbol{\xi}, \lambda_0)$ to be a solution of (2.14) periodic in ξ_1 with boundary conditions

$$V_1^{(2)}|_{\xi_2=1} - V_1^{(2)}|_{\xi_2=-1} = 2U_0|_{\xi_2=1} \quad (2.17)$$

$$V_{1\xi_2}^{(2)}|_{\xi_2=1} - V_{1\xi_2}^{(2)}|_{\xi_2=-1} = 2U_{0\xi_2}|_{\xi_2=1}. \quad (2.18)$$

The second order equation for $u_2(\mathbf{X}, \boldsymbol{\xi})$ is

$$\begin{aligned} &\nabla_{\boldsymbol{\xi}} \cdot [a(\boldsymbol{\xi}) \nabla_{\boldsymbol{\xi}} u_2] + \lambda_0^2 \rho(\boldsymbol{\xi}) u_2 \\ &\quad = -a(\boldsymbol{\xi}) U_0 \nabla_{\mathbf{X}}^2 f_0 - [2a(\boldsymbol{\xi}) \nabla_{\boldsymbol{\xi}} + \nabla_{\boldsymbol{\xi}} a(\boldsymbol{\xi})] \cdot \nabla_{\mathbf{X}} u_1 - \lambda_2^2 \rho(\boldsymbol{\xi}) f_0 U_0 \end{aligned} \quad (2.19)$$

and this contains both $f_0(\mathbf{X})$ and the correction, λ_2^2, to the eigenvalue λ_0^2. Invoking an orthogonality condition, as at the previous order, by multiplying (2.19) by U_0, subtracting (2.7) times u_2/f_0 from it, and integrating the result over the cell yields an eigenvalue problem for f_0 and λ_2^2 as the homogenized partial differential equation

$$T_{ij}\frac{\partial^2 f_0}{\partial X_i \partial X_j} + \lambda_2^2 f_0 = 0, \quad \text{with} \quad T_{ij} = \frac{t_{ij}}{\iint_S \rho(\boldsymbol{\xi}) U_0^2 dS} \quad \text{for} \quad i,j = 1,2. \tag{2.20}$$

The components of the matrix t_{ij} given by

$$t_{11} = -2\int_{-1}^{1} [a(\boldsymbol{\xi})U_0^2]_{\xi_1=1} d\xi_2 + \iint_S (2a(\boldsymbol{\xi})V_{1\xi_1}^{(1)} + a_{\xi_1}(\boldsymbol{\xi})V_1^{(1)})U_0 dS, \tag{2.21}$$

$$t_{12} = t_{21} = \frac{1}{2}\iint_S \left(2a(\boldsymbol{\xi})(V_{1\xi_2}^{(1)} + V_{1\xi_1}^{(2)}) + a_{\xi_2}(\boldsymbol{\xi})V_1^{(1)} + a_{\xi_1}(\boldsymbol{\xi})V_1^{(2)}\right) U_0 dS, \tag{2.22}$$

$$t_{22} = -2\int_{-1}^{1} [a(\boldsymbol{\xi})U_0^2]_{\xi_2=1} d\xi_1 + \iint_S (2a(\boldsymbol{\xi})V_{1\xi_2}^{(2)} + a_{\xi_2}(\boldsymbol{\xi})V_1^{(2)})U_0 dS. \tag{2.23}$$

Thus given a particular structure we solve the leading order equation (2.7) to determine λ_0, $U_0(\boldsymbol{\xi}, \lambda_0)$. Then solve (2.14), with boundary conditions (2.15)-(2.18) and periodicity, to find $\mathbf{V}_1(\boldsymbol{\xi}, \lambda_0)$. Given these quantities the differential eigenvalue problem (2.20) is formed, and thus λ_2 identified.

We now specialize to one-dimensional, or quasi-one-dimensional problems for which this scheme is more readily applied and for which some explicit details are immediately apparent.

(*a*) *One-dimensional periodic media*

Assuming $a(\xi)$ is constant, then for one-dimensional structures (2.2) simplifies to

$$l^2\frac{d^2u}{dx^2} + \lambda^2\frac{u}{c^2(\xi)} = 0, \qquad \text{with} \quad \lambda = \frac{\omega l}{\hat{c}_0}. \tag{2.24}$$

where we define $c^2(\xi) = a/\rho(\xi)$. The assumption that $a(\xi)$ is constant in (2.24) is not essential as any homogeneous second order differential equation can be transformed into this form by an appropriate change of variables.

The independent variables are now $X = x/L, \xi = x/l$ and the solution $u(X,\xi)$ will be periodic, or anti-periodic, in ξ, but not necessarily in X. The two-scales approach yields

$$\frac{\partial^2 u}{\partial \xi^2} + 2\varepsilon\frac{\partial^2 u}{\partial \xi \partial X} + \varepsilon^2\frac{\partial^2 u}{\partial X^2} + \frac{\lambda^2}{c^2(\xi)}u = 0\,. \tag{2.25}$$

This equation is solved subject to either ξ-periodicity conditions $u(X,1) = u(X,-1)$ and $u_\xi(X,1) = u_\xi(X,-1)$ or, what we have named, anti-periodicity conditions $u(X,1) = -u(X,-1)$ and $u_\xi(X,1) = -u_\xi(X,-1)$, which actually result in the solutions being ξ-periodic across two cells. As we shall see shortly, these two cases correspond to standing waves that are either in-phase or completely out-of-phase at the end of each cell and, in Floquet-Bloch theory, to wave numbers situated at the opposite ends of the Brillouin zone.

The separation of scales is loosely analogous to the long-wave high frequency asymptotics outlined for infinite, deformed, waveguides (Berdichevski, 1983; Kaplunov *et al.*, 1998; Le, 1999) and this analogy can be pursued to obtain a physical interpretation of the results and this is discussed in sections 2(b) and 4. As in the two-dimensional theory we form a hierarchy of equations to be solved order-by-order. To leading order:

$$u_{0\xi\xi} + \frac{\lambda_0^2}{c^2(\xi)} u_0 = 0 \tag{2.26}$$

and if λ_0 is a simple eigenvalue of the problem with an appropriate set of boundary conditions, then

$$u_0(\xi, X) = f_0(X) U_0(\xi, \lambda_0). \tag{2.27}$$

In the periodic case $U_0(1, \lambda_0) = U_0(-1, \lambda_0)$, $U_{0\xi}(1, \lambda_0) = U_{0\xi}(-1, \lambda_0)$ and in the anti-periodic case $U_0(1, \lambda_0) = -U_0(-1, \lambda_0)$, $U_{0\xi}(1, \lambda_0) = -U_{0\xi}(-1, \lambda_0)$. From Floquet theory, all band gaps present in the Bloch spectra of (2.26) are bound by the eigenvalues corresponding to periodic or anti-periodic solutions. Hence, the high frequency asymptotics developed here are expected to provide accurate description of the solution's band gap structure in a wide range of problems.

To next order:

$$u_{1\xi\xi} + \frac{\lambda_0^2}{c^2(\xi)} u_1 = -2u_{0\xi X} - \frac{\lambda_1^2}{c^2(\xi)} u_0 \tag{2.28}$$

with the compatibility condition giving $\lambda_1 = 0$. The solution is

$$u_1(X, \xi) = f_{0X} \left[A W_1(\xi, \lambda_0) - \xi U_0(\xi, \lambda_0) \right] + f_1(X) U_0(\xi, \lambda_0) \tag{2.29}$$

where $W_1(\xi, \lambda_0)$ is a non-periodic solution of the leading order equation and

$$A = \frac{2U_0(1, \lambda_0)}{W_1(1, \lambda_0) \mp W_1(-1, \lambda_0)} \tag{2.30}$$

with the upper (lower) sign being for the periodic (anti-periodic) case and the constant A is chosen to enforce that behaviour. At next order:

$$u_{2\xi\xi} + \frac{\lambda_0^2}{c^2(\xi)} u_2 = -\frac{\lambda_2^2}{c^2(\xi)} u_0 - u_{0XX} - 2u_{1\xi X} \tag{2.31}$$

with the compatibility condition giving

$$T f_{0XX} + \lambda_2^2 f_0 = 0 \tag{2.32}$$

where the coefficient T is

$$T = 2 \left(\frac{-U_0^2(1, \lambda_0) + A \int_{-1}^{1} U_0 W_{1\xi} d\xi}{\int_{-1}^{1} U_0^2 / c^2(\xi) d\xi} \right). \tag{2.33}$$

The differential eigenvalue problem (2.32) then encapsulates the essential physics and the correction to the frequency squared, λ_2^2, is its eigenvalue.

If the leading order solution has $U_0(\pm 1, \lambda_0) = 0$ then (2.29) is not valid, however this is easy to overcome with (2.33) replaced by

$$T = \frac{2A \int_{-1}^{1} U_0 W_{1\xi} d\xi}{\int_{-1}^{1} U_0^2 / c^2(\xi) d\xi} \tag{2.34}$$

where $A = 2U_{0\xi}(1,\lambda_0)/[W_{1\xi}(1,\lambda_0) \mp W_{1\xi}(-1,\lambda_0)]$ and the non-periodic function W_1 satisfies the Dirichlet conditions, $W_1(\pm 1,\lambda_0) = 1$ (or any non-zero constant).

A degeneracy occurs whenever λ_0 is not a simple eigenvalue, as the leading order solution (2.26) must consist of two linearly independent periodic solutions:

$$u_0(\xi, X) = f_0^{(1)}(X)U_0^{(1)}(\xi,\lambda_0) + f_0^{(2)}(X)U_0^{(2)}(\xi,\lambda_0). \tag{2.35}$$

The compatibility condition for the first order term then gives two coupled ODEs for $f_0^{(1,2)}$ from which the eigenvalue correction λ_1^2 is obtained; the correction to the eigenvalue is now linear rather than quadratic. The coupled equations are

$$f_{0X}^{(i)} \int_{-1}^{1} U_0^{(j)} U_{0\xi}^{(i)} d\xi + \lambda_1^2 \int_{-1}^{1} \left(f_0^{(j)} U_0^{(j)2} + f_0^{(i)} U_0^{(i)} U_0^{(j)} \right) \frac{d\xi}{c^2(\xi)} = 0 \tag{2.36}$$

for $i, j = 1, 2$ and $j \neq i$.

The asymptotic model (2.32) is not uniform in the sense that when material parameters are continuously varied, such that two eigenvalues approach one another, one has then to switch to the model equations (2.36). Examples from waveguide theory suggest that it is possible to construct uniformly valid composite expansions (Moukhomodiarov *et al.*, 2010) to overcome this.

(*b*) *Analogy with homogeneous waveguides*

Placing equation (2.32) in dimensional form

$$l^2 T \frac{d^2 f_0}{dx^2} + (\lambda^2 - \lambda_0^2) f_0 = 0 \tag{2.37}$$

then this equation governs the 1D long wave motion of a periodic medium near the resonance frequencies of a cell. It may be subject to macroscopic boundary conditions along the edges and may also involve inhomogeneous terms on the right-hand side corresponding to edge and surface loadings, see Kaplunov *et al.* (1998) and references therein.

The long wave equation (2.37) may be interpreted as describing a homogeneous string attached to an elastic foundation. Although the microscale problem is governed by a Helmholtz equation with periodic coefficients, (2.24), the proposed model cannot be formally identified as a Helmholtz equation with an averaged wave speed, which contrasts with traditional homogenization theory. At the same time the model does not contain microscale variables operating only with long-scale phenomena. It is worth noting that non-local equations are also known to occur as homogenized limits for certain high-contrast composite media (Cherednichenko *et al.*, 2006).

As we have mentioned earlier, the model represents an analogue of the high frequency long wave theories for elastic and acoustic homogeneous waveguides (e.g. Kaplunov *et al.* (1998); Gridin *et al.* (2005)). In fact, the problem on a cell (2.26) corresponds to one on the transverse cross-section of a thin rod, plate or a shell. In this case the cell size l in (2.24) corresponds to the half-thickness and the cell eigenvalue λ_0 corresponds to a thickness resonance frequency. A similar analogy also occurs in conventional homogenization theory which is, in a sense, a counterpart of the classical low frequency theories for rods, plates and shells associated with the names of Euler, Bernoulli, Kirchhoff and Love (e.g. Graff, 1975; Landau & Lifshitz, 1970; Love, 1944). The discussion above is also applicable to 2D periodic media.

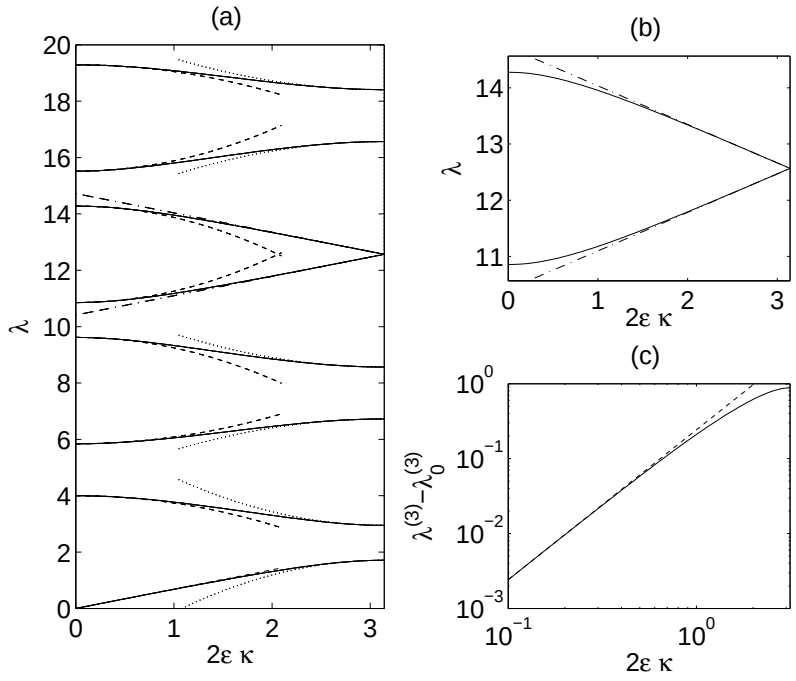

Figure 2. The dispersion curves from (3.2), for $r = 1/4$, shown across the Brillouin zone in panel (a). The solid line is from the numerical solution, the asymptotics for $\kappa \to 0$ are the dashed curve and for $2\varepsilon\kappa \to \pi$ are dotted. Asymptotics for the double root are shown as dot-dashed lines. Panel (b) shows the detail for the Bloch spectra at the double root at $\lambda_\pi^{(4)} = \lambda_\pi^{(5)} = 4\pi$ with the asymptotics shown as the dot-dashed lines. Panel (c) plots $\lambda^{(3)} - \lambda_0^{(3)}$ on log-log axes to illustrate the accuracy: numerics are given by the solid line and the asymptotics are the dashed line.

3. Illustrative examples

To illustrate the efficacy of this approach we turn our attention to some examples. The first example, a periodic piecewise homogeneous material, has the advantage of being explicitly solvable and serves to illustrate typical features of Bloch waves and pass-stop bands in periodic media. For some parameters, double roots occur allowing this feature to also be explored. This example is extended by introducing a parameter leading to the formation of a low frequency stop band, hence allowing us to compare and contrast the high frequency theory with a traditional low frequency homogenization. Our last example is of a string with a periodic density that leads to Mathieu's equation, allowing us to present a non-trivial application of our asymptotics.

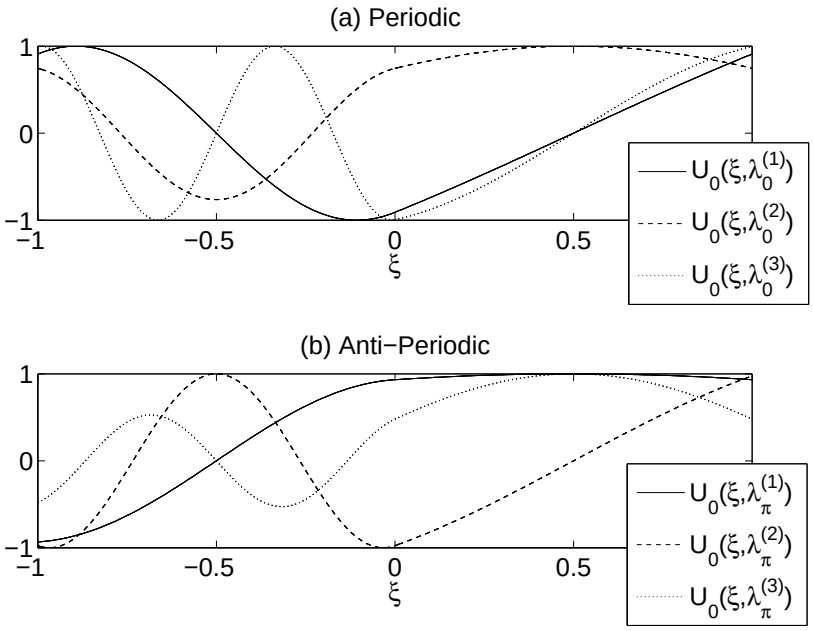

Figure 3. The leading order solutions U_0 for $\lambda^{(1)}$, $\lambda^{(2)}$, $\lambda^{(3)}$ from Figure 2 shown in panel (a) at the $\kappa = 0$ edge of the Brillouin zone and in (b) at the $2\varepsilon\kappa = \pi$ edge.

(*a*) *Periodic piecewise homogeneous media*

For a material with piecewise constant variation in $c(\xi)$:

$$c(\xi) = \begin{cases} 1/r & \text{for} \quad 0 \le \xi < 1 \\ 1 & \text{for} \quad -1 \le \xi < 0 \end{cases} \tag{3.1}$$

for r a positive constant, an exact solution is readily obtained. Floquet-Bloch conditions (Brillouin, 1953; Kittel, 1996) are set at $\xi = \pm 1$ so $u(1) = \exp(i2\kappa\varepsilon)u(-1)$ and $u_\xi(1) = \exp(2i\kappa\varepsilon)u_\xi(-1)$, the solution and its derivatives are continuous at $\xi = 0$, and κ is the Bloch parameter. The dispersion relation relating frequency, λ, to Bloch parameter, κ, is

$$2r[\cos\lambda\cos r\lambda - \cos 2\varepsilon\kappa] - (1 + r^2)\sin\lambda\sin r\lambda = 0. \tag{3.2}$$

This dispersion relation was seemingly first obtained by Kronig & Penney (1931) for electrons in crystal lattices; it also naturally appears in many guises in one dimensional photonic and phononic crystals (with layers of infinite height), see e.g. Movchan *et al.* (2002); Adams *et al.* (2008). There are an infinite number of discrete eigenfrequencies, $\lambda(\kappa)$, to the dispersion relation which we denote as $\lambda^{(n)}$ with $n = 0, 1, 2...$ ordered from the lowest curve upward, typical Bloch spectra are shown in Figure 2. The asymptotic technique we describe extracts the behaviour of the dispersion curves near $\lambda_0^{(n)}$, which is the frequency at the edge of the Brillouin zone where $\kappa = 0$. The standing waves that occur when $\kappa = 0$ correspond to solutions periodic across each elementary cell of width 2ε. The other end of the Brillouin

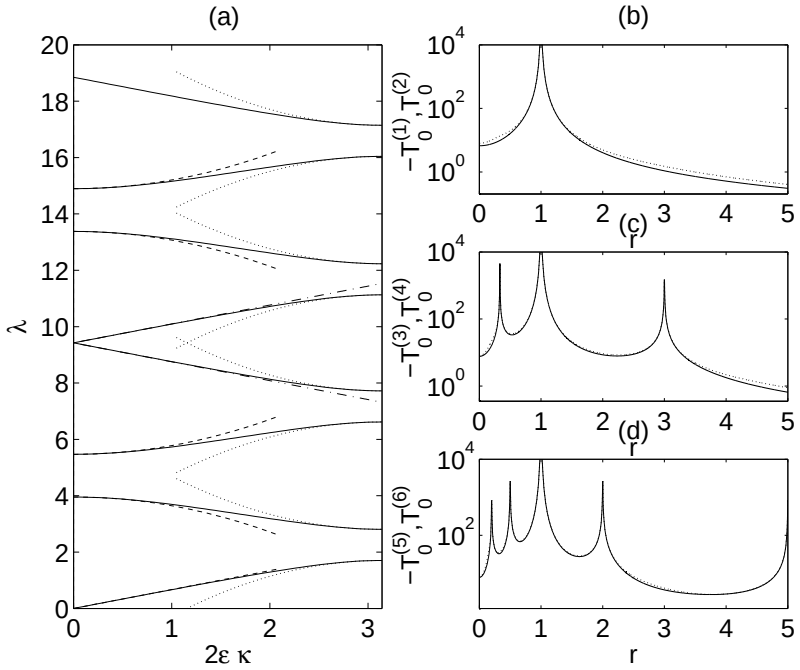

Figure 4. The dispersion curves from (3.2), for $r = 1/3$, shown across the Brillouin zone in (a); the asymptotic solution is the dashed curve whilst the numerical solution of the exact dispersion relation is the solid curve. This figure shows the presence of a double root for $\lambda_0 = 3\pi \sim 9.42$ and the asymptotics for this degenerate case come from (3.9). Panels (b)-(d) show $T_0^{(n)}$ versus r for $n = 1..6$. Even (odd) n are positive (negative), and dotted (solid) lines which are almost indistinguishable in each pairing on the scale shown.

zone is at $2\varepsilon\kappa = \pi$ and correspond to standing waves out-of-phase across the cell, the anti-periodic solutions which are periodic on a double cell, and the frequencies at which these occur are denoted by $\lambda_\pi^{(n)}$. The asymptotics we develop are valid near each $\lambda_\pi^{(n)}$ and all $\lambda_0^{(n)}$ except the low frequency fundamental mode passing through $\lambda_0^{(0)} = 0$. This mode is the one described by classical homogenization, whose characterization is straightforward, $\lambda_0^{(0)} \sim 2\varepsilon\kappa/\sqrt{2(1+r^2)}$ c.f. (3.14), at $\beta = 0$, which corresponds to the substitution

$$\left\langle \frac{1}{c^2} \right\rangle = \frac{1}{2}\int_{-1}^{1} \frac{1}{c^2(\xi)} d\xi \tag{3.3}$$

in (2.24). We compare the classical philosophy with the high frequency theory at the end of Section 3b.

We now turn to the asymptotic procedure. The leading order solution is determined as

$$U_0(\xi, \lambda_\theta^{(n)}) = \begin{cases} \sin r\lambda_\theta^{(n)}\xi + p\cos r\lambda_\theta^{(n)}\xi & \text{for} \quad 0 \le \xi < 1 \\ r\sin \lambda_\theta^{(n)}\xi + p\cos \lambda_\theta^{(n)}\xi & \text{for} \quad -1 \le \xi < 0 \end{cases} \tag{3.4}$$

for $\lambda_\theta^{(n)} = \lambda_0^{(n)}, \lambda_\pi^{(n)}$ and $p = (r\sin\lambda_\theta^{(n)} \pm \sin r\lambda_\theta^{(n)})/(\cos\lambda_\theta^{(n)} \mp \cos r\lambda_\theta^{(n)})$ with the upper, lower signs for $\theta = 0, \pi$ respectively. We also need a linearly independent solution, which does not satisfy periodicity or anti-periodicity conditions at $\xi = \pm 1$, $W_1(\xi, \lambda_\theta^{(n)})$. We take it as

$$W_1(\xi, \lambda_\theta^{(n)}) = \begin{cases} \sin r\lambda_\theta^{(n)}\xi & \text{for} \quad 0 \le \xi < 1 \\ r\sin\lambda_\theta^{(n)}\xi & \text{for} \quad -1 \le \xi < 0. \end{cases} \tag{3.5}$$

Note that W_1 can be taken to be *any* solution of the leading order equation with fixed λ_0 which is neither periodic nor anti-periodic. Once W_1 is found it can be re-used in the asymptotics for either end of the Brillouin zone.

Substituting these into (2.33) gives T_0 and T_π, that is, the T values associated with the periodic and anti-periodic solutions. These two are written using a single formula as

$$T_\theta^{(n)} = \pm 4\lambda_\theta^{(n)} \frac{\sin\lambda_\theta^{(n)} \sin\lambda_\theta^{(n)} r}{(r\sin\lambda_\theta^{(n)} \mp \sin r\lambda_\theta^{(n)})(\cos\lambda_\theta^{(n)} \mp \cos r\lambda_\theta^{(n)})} \tag{3.6}$$

where we append a subscript to T to denote its dependence upon $\lambda_\theta^{(n)}$ and $T_0^{(n)}$ ($T_\pi^{(n)}$) is the value with the upper (lower) sign and $\lambda_\theta^{(n)} = \lambda_0^{(n)}(\lambda_\pi^{(n)})$.

We now turn our attention to the ODE for f_0, namely (2.32), and note that the Floquet-Bloch conditions lead to $u(X + 2\varepsilon, \xi) = \exp(2i\varepsilon\kappa)u(X, \xi)$. For the periodic case in ξ this forces $f_0(X) = \exp(i\kappa X)$. Thus we connect the Bloch parameter with the frequency, found from (2.32), via $T\kappa^2 = \lambda_2^{(n)2}$ and deduce that

$$\lambda^{(n)} \sim \lambda_0^{(n)} + \frac{\varepsilon^2}{2}\frac{\lambda_2^{(n)2}}{\lambda_0^{(n)}} + ... = \lambda_0^{(n)} + \frac{\varepsilon^2}{2}\frac{T_0^{(n)}\kappa^2}{\lambda_0^{(n)}} + ... \tag{3.7}$$

Similarly in the anti-periodic case we deduce $f_0(X) = \exp(i(\kappa - \pi)X)$ and

$$\lambda^{(n)} \sim \lambda_\pi^{(n)} + \frac{\varepsilon^2}{2}\frac{T_\pi^{(n)}(\kappa - \pi)^2}{\lambda_\pi^{(n)}} + ... \tag{3.8}$$

The same results are found directly by expanding the exact dispersion relation (3.2) thereby validating the asymptotic scheme for an example that can be explicitly analyzed; the advantage of the asymptotic procedure is that it is applicable even when the dispersion relation is unwieldy or unavailable. Since the derived expansion makes no specific assumptions about the form of the leading order solution, it is valid for arbitrary volume fractions, although the resulting numerical accuracy at fixed wavenumbers may vary.

We order the eigenvalues for $n = 0...\infty$ from lowest to highest in magnitude and note that the asymptotics do not apply to the lowest eigenvalue, $\lambda_0^{(0)}$, which passes through the origin and which have been approached separately, but is accurate for high frequencies. Figure 2 shows the band gap structure and associated asymptotics that emanate from the frequencies at the edges of the Brillouin zone. The quadratic corrections are highly accurate even for values of κ far away from the edges of the zone and this is shown in Figure 2(c). A double root occurs at $\lambda_\pi^{(4)} = \lambda_\pi^{(5)}$ and

the asymptotics shown in Figure 2(b) are the linear corrections from (2.36). An essential ingredient of the asymptotic procedure is the identification of the leading order solutions $U_0(\xi, \lambda_\theta^{(n)})$ for the standing waves across the structure. Typical curves are shown in Figure 3 for the U_0 at each edge of the Brillouin zone, as the frequency increases the solutions gain more spatial structure.

The degenerate case of a double root is again illustrated in Figure 4. In Figure 4(b) we note that $T_0^{(n)}$ diverges for some values of r and further analysis shows that these values correspond to the cases of a double root for $\lambda_\theta^{(n)}$ which occur whenever $r = 1/m, m$ (for integer m). For instance, for $r = 1/3$, as in the figure, $\lambda_0^{(4),(5)} = 3\pi$, and there is no band gap (as shown in Figure 4(a)). The asymptotics are extracted using the coupled equations (2.36) as

$$\lambda^{(3),(4)} \sim 3\pi \pm \frac{3\varepsilon\kappa}{\sqrt{5}} + \dots \tag{3.9}$$

and as noted earlier the correction is linear in κ rather than the quadratic behaviour found for distinct roots. A similar double root behaviour occurs at the other end of the Brillouin zone, and is shown in Figure 2(b), together with the asymptotics from (2.36).

(*b*) *A model structure with non-uniform low frequency behaviour*

The piecewise homogeneous structure has its lowest Bloch spectra curve $\lambda^{(0)}(\kappa)$ passing through $\lambda^{(0)}(0) = \lambda_0^{(0)} = 0$ and as it passes exactly through zero this low frequency mode is not captured within our asymptotics. Classical homogenization theory describes the behaviour of this low frequency curve both when it passes through zero and when an extra (small) parameter exists, as in the example to be considered in this section, that moves the curve upward to expose a low frequency stop band. We now consider an adaption of the piecewise homogeneous model that allows us to contrast the classical theory with our high frequency asymptotic approach for this lowest curve of the Bloch spectra.

We previously mentioned that the model equations obtained during the high frequency homogenization of one-dimensional periodic structures describes vibration of an effective homogeneous string on a Winkler foundation. In this context, it is instructive to study homogenization of a periodically piecewise homogeneous string on a Winkler foundation. This setup also describes a striped waveguide (Adams *et al.*, 2008, 2009) of finite thickness with Dirichlet, Neumann or impedance (Robin) boundary conditions along the guide walls. In both cases the governing equation is equivalent to

$$l^2 \frac{d^2u}{dx^2} - \beta^2 u + \frac{\lambda^2}{c^2(x/l)} u = 0. \tag{3.10}$$

The additional term $-\beta^2 u$ corresponds to the constant elastic restoring parameter in the Winkler model, or to the separation constant which is related to the transverse mode number for the striped waveguide, and its presence creates a low frequency stop band. The dispersion relation is a minor adjustment of (3.2) to

$$2k_1k_2(\cos k_1 \cos k_2 - \cos 2\varepsilon\kappa) - (k_1^2 + k_2^2) \sin k_1 \sin k_2 = 0 \tag{3.11}$$

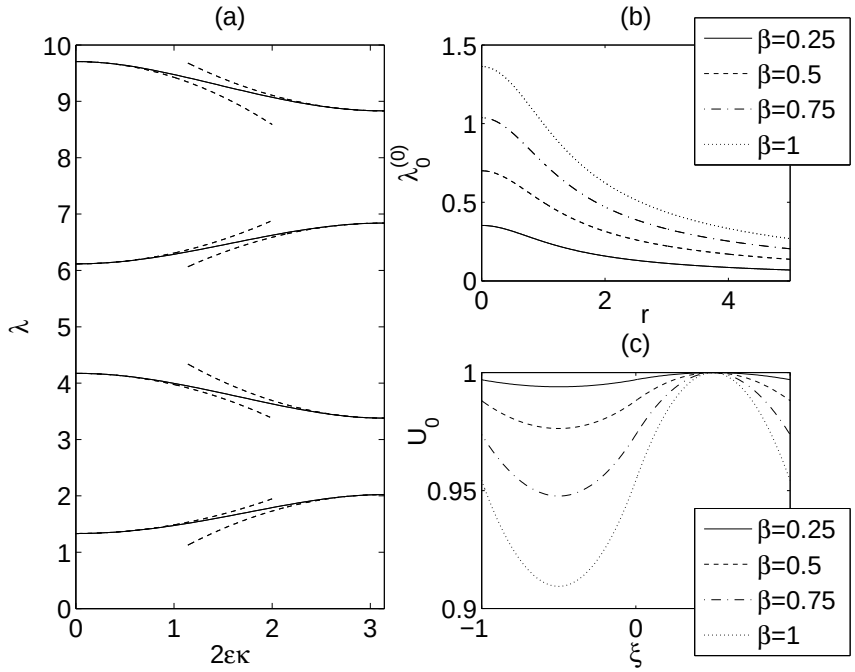

Figure 5. The dispersion curves for the piecewise homogeneous string on a Winkler foundation. Panel (a) is for $r = 1/4$, $\beta = 1$ showing the absence of the fundamental mode and the curves from the full numerics (solid) versus the asymptotics (dashed). Panel (b) shows the variation of the lowest frequency cut-off at $\kappa = 0$, namely $\lambda_0^{(0)}$, versus the change in wavespeed r for various values of β. Panel (c) shows the variation in the leading order solution, $U_0(\xi, \lambda_0^{(0)})$ as β increases for fixed r: $r = 1.5$ in panel (c).

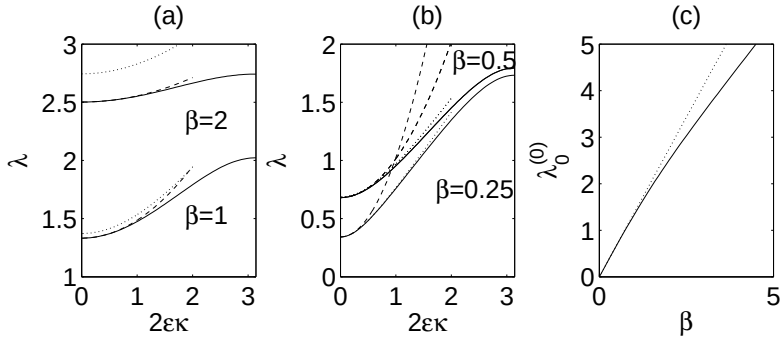

Figure 6. A comparison of the low frequency homogenization formula (3.14) (dotted lines) with the numerical solution (solid) and the high frequency asymptotics (dashed). In all panels $r = 1/4$ and in panel (a) we show $\lambda^{(0)}$ for $\beta = 2$ and $\beta = 1$. Likewise in panel (b) but for $\beta = 0.5$ and $\beta = 0.25$. Panel (c) shows the variation in $\lambda_0^{(0)}$ versus β predicted by the low frequency asymptotics (dotted) and from the numerics (solid).

with $k_1^2 = \lambda^2 - \beta^2$, $k_2^2 = r^2\lambda^2 - \beta^2$. For non-zero β there is no fundamental mode passing through the origin in the Bloch spectra for this model, hence high-frequency asymptotics are capable of describing every Floquet-Bloch mode. The two scales analysis goes through precisely as before with $\lambda_0^{(n)}$ deduced from (3.11) with $\kappa = 0$. The asymptotic correction $\lambda_2^{(n)}$ is deduced from (2.32) by integrating the leading order solution U_0 and the associated W_1 to find $T^{(n)}$ from (2.33). Results for typical values are shown in figure 5. Importantly there is no curve passing through the origin and the lowest curve cuts the frequency axis at $\lambda_0^{(0)}$. The variation of $\lambda_0^{(0)}$ versus change in wave speed, r, is shown in figure 5(b) for various β. When $\beta = 0$, $\lambda_0^{(0)} = 0$ always and the curve then passes through the origin and is a conventional low frequency mode. As β increases the curves move away from the r axis and there is always a low frequency band gap bounded above by $\lambda_0^{(0)}$. If $\beta = 0$ then the leading order solution $U_0 = U(\xi, \lambda_0^{(0)})$ is just a flat line, that is it has no spatial structure and is the state that one would use in classical homogenization, and as β increases, the mode-shape varies and begins to take on more structure; the curves in figure 5(c) are normalized to have $\max(|U_0|) = 1$. Further details of the Bloch spectra for this example are in Adams *et al.* (2008, 2009) together with details of numerical schemes and other asymptotic techniques that can be applied.

The lowest curve of the Bloch spectra can be approximated using quasi-static distributions along the cell corresponding to classical homogenization. This requires low frequencies and $\beta \sim \varepsilon\hat{\beta}$ for which the appropriate asymptotic ordering is that

$$u(X,\xi) = u_0(X,\xi) + \varepsilon u_1(X,\xi) + \ldots, \qquad \lambda^2 = \varepsilon^2\lambda_2^2 + \ldots. \tag{3.12}$$

The leading order equation then gives $u_0(X,\xi) = f_0(X)$ which is uniform along the cell, that is, it does not depend upon the small-scale ξ at all and this difference, and the scaling of λ, are a major difference between the high and low frequency models. The function $f_0(X)$, from the second order equation, satisfies the differential eigenvalue problem

$$f_{0XX} - \hat{\beta}^2 f_0 + f_0 \frac{\lambda_2^2}{2} \int_{-1}^{1} \frac{1}{c^2(\xi)} d\xi = 0. \tag{3.13}$$

In this classical model the inverse squared wave speed c is replaced in (3.10) by an averaged quantity $< 1/c^2 >$, defined in (3.3), and homogenization replaces the variable wave speed by this averaged quantity. The high frequency asymptotics that we employ are fundamentally different, they are not limited by low frequency quasi-static variations along the cell and do not simply replace periodic inverse wave speed squared by a constant. The asymptotics take the solution of the standing wave and construct an effective parameter, T, as an integral over ξ that involves the wave speed and the standing wave solution.

Returning to the problem at hand, the Bloch conditions yield $f_0(X) = \exp(i\kappa X)$ and thus this lowest curve is given asymptotically in the low frequency limit as

$$\lambda^{(0)2} \sim \frac{4\beta^2 + (2\varepsilon\kappa)^2}{2(1+r^2)} \tag{3.14}$$

for $\beta \ll 1$ and small κ. We compare this result with the high frequency asymptotics in figure 6, from panels (b) and (c) we see that at low frequencies, equivalently small

β, (3.14) performs well predicting both the changes in frequency when $\kappa = 0$ and in predicting $\lambda^{(0)}$. The high frequency results are applicable for small κ but diverge from the numerics sooner than the low frequency results. For large β, figure 6(a), the low frequency theory drifts away from the solid curve, and becomes inaccurate, and the high frequency results remain accurate and are so over a longer domain in κ.

(*c*) *A continuous periodic variation*

We now consider a string with periodic variation in density that leads to the wave speed $c^{-2}(\xi) = \alpha - 2\Theta\cos 2\xi$, where α, Θ are positive constants; this variation gives the classical Mathieu equation (McLachlan, 1964; Abramowitz & Stegun, 1964) and to more readily connect with the standard theory for that equation we choose the period to be $\pi\varepsilon$ rather than 2ε. To obtain the Bloch spectrum the Mathieu equation

$$u_{\xi\xi} + \lambda^2(\alpha - 2\Theta\cos 2\xi)u = 0 \tag{3.15}$$

is solved with Floquet-Bloch conditions at $\xi = 0, \pi$ namely $u(\pi) = \exp(i\pi\kappa\varepsilon)u(0)$ and $u_\xi(\pi) = \exp(i\pi\kappa\varepsilon)u_\xi(0)$. The resulting differential eigenvalue problem for λ is solved numerically using a spectral collocation scheme with Chebyshev basis functions (Adams *et al.*, 2008; Weideman & Reddy, 2000) and a typical Bloch spectrum is shown in figure 7. In the language associated with Mathieu's equation κ is the characteristic exponent and $\lambda^2\alpha, \lambda^2\Theta$ are usually denoted as a, q; usually the characteristic exponent is found in terms of fixed a, q whereas in the current application this is reversed with κ known, (and α, Θ known) but with λ^2 to be determined.

The periodic and anti-periodic leading order solutions $U_0(\xi, \lambda_0^{(n)})$ and $U_0(\xi, \lambda_\pi^{(n)})$ are extracted numerically for $\kappa = 0, \pi$ respectively and W_1 is determined as a non-periodic solution of (3.15). In the periodic case the leading order solutions fall into the two linearly independent solutions described in Section 20.3 of Abramowitz & Stegun (1964). One being characterized by $U_0(0, \lambda_0^{(n)}) = 1$, $U_0(\pi, \lambda_0^{(n)}) = 1$, $U_{0\xi}(\pi, \lambda_0^{(n)}) = 0$ (these lead to the n odd cases) and the other by $U_{0\xi}(0, \lambda_0^{(n)}) = 1$, $U_{0\xi}(\pi, \lambda_0^{(n)}) = 1$, $U_0(\pi, \lambda_0^{(n)}) = 0$ (these lead to the n even cases). The n even cases have $U_0(\pi, \lambda_0^{(n)}) = 0$ and the formula for T from (2.34) is utilized. The non-periodic solution W_1 is taken to have boundary conditions $W_1(0, \lambda_0^{(n)}) = 0, W_1(\pi, \lambda_0^{(n)}) = 1$ for the odd case and $W_1(0, \lambda_0^{(n)}) = W_1(\pi, \lambda_0^{(n)}) = 1$ for the even case. The anti-periodic case also naturally falls into two linear independent solutions and these too are found numerically.

Given the leading order, U_0, and non-periodic, W_1, solutions the integrals for T are evaluated numerically. The change of length of the periodic domain leads to minor changes due to a rescaling of the domain and after performing this change, the corrections $\lambda_2^{(n)}$ to $\lambda_0^{(n)}$ and $\lambda_\pi^{(n)}$ are readily found and the resulting asymptotics are shown versus the complete numerics in figure 7. The asymptotics are highly accurate near the edges of the Brillouin zone as illustrated in Figure 7(a). The curve for $\lambda^{(0)}$ passes through the origin and the asymptotics for this curve near zero are found using the classical low frequency approach, as in (3.13), and $\lambda^{(0)} \sim \varepsilon\kappa/\sqrt{\alpha}$.

The leading order solutions for U_0 are shown in figure 7(b) with the $n = 2$ solution clearly zero at the ends of the domain, and the solutions chosen for W_1 are

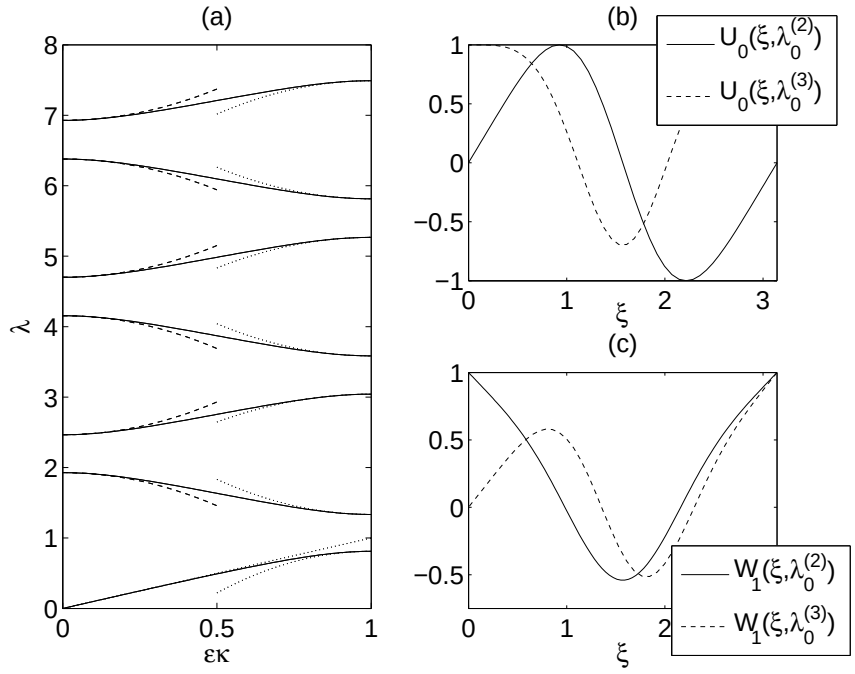

Figure 7. The dispersion curves for Mathieu's equation for $\alpha = 1, \Theta = 1/2$, shown across the Brillouin zone in panel (a); the asymptotic solution from $\lambda_0^{(n)}$ at the $\kappa = 0$ edge of the Brillouin zone is the dashed curve, the asymptotics from $\kappa = \pi$ are the dotted curve, whilst the numerical solution is the solid curve. Panels (b) and (c) show the leading order solutions for $U_0(\xi, \lambda_0^{(n)})$ and $W_1(\xi, \lambda_0^{(n)})$ respectively for $n = 2, 3$.

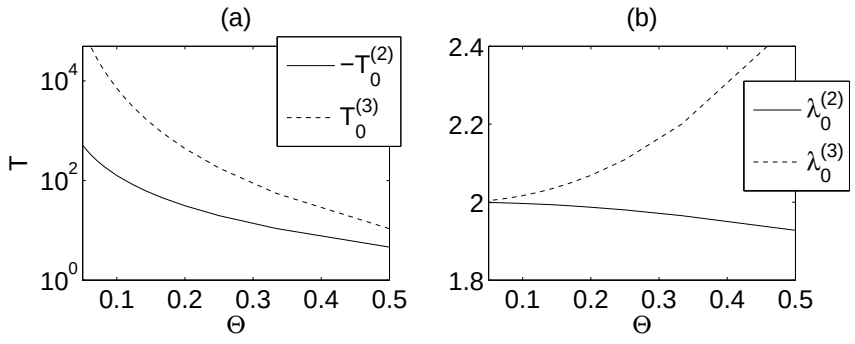

Figure 8. Panels (a) and (b) show the variation of $T_0^{(n)}$ and $\lambda_0^{(n)}$ versus Θ, for $\alpha = 1$, for $n = 2, 3$.

shown in figure 7(c). Panels (a) and (b) of Figure 8 show that as $\Theta \to 0$, physically the material variation decreasing, the values of $T_0^{(n)}$ shown increase dramatically and the difference between the consecutive $\lambda_0^{(n)}$ decrease until the band gap disap-

pears and one obtains a double root; the figure shows the results for $n = 2, 3$ and similar results hold for higher n and at the other end of the Brillouin zone.

4. Concluding remarks

The high frequency asymptotic theory that we present extends classical homogenization, breaking free of the static and low frequency limitation on the solution variation along the cell. The examples chosen show that by perturbing away from the standing wave solutions, the Bloch spectra are identified through a simple differential eigenvalue problem (2.20) in 2D and (2.32) in 1D. This differential eigenvalue problem is characterized by a constant parameter whose definition involves the integrations over the short-scale of the periodic cell and this short-scale plays no further role in the problem; the methodology differs from conventional homogenization theory is several critical ways, the main one is that the basic state has spatial dependence and so the integrated quantities are not simply averaged wavespeeds or simple averaged quantities.

Remarkably the final ODE (2.32) is exactly that which arises in the high frequency long-wave asymptotics in, say, a straight acoustic waveguide (Gridin *et al.*, 2004). Near the thickness resonance frequencies for the waveguide, i.e. near the eigenvalues of the transverse resonance problem for a homogeneous waveguide, a wave bounces across the guide width forming a near-standing wave that barely propagates along the guide. Therefore despite being at high frequency the wavelength is long. In the periodic situation considered in this article the vision we have of the wave is that it bounces within a periodic cell of the structure with no phase change, or complete phase change, across the period, to leading order, again forming a standing wave barely propagating along the structure. In both situations, the transverse resonance and standing waves, the wave about which we perturb has large wavelength, but can occur at high frequency and so they are both amenable to similar asymptotic methods. A major benefit of having an asymptotic theory to hand is that it uncovers the physics and also complements numerical schemes. For instance, by evaluating the parameter T directly from the standing wave solutions it is possible to both determine the sign and, estimate the value, of group velocity of Bloch modes near the edges of the Brillouin zone.

In the long-wave high frequency theory of waveguides the ODE is often augmented by terms that account for curvature or geometrical variations along the guide (Kaplunov *et al.*, 2005; Gridin *et al.*, 2005) and which may lead to trapping or localisation phenomena. Similar adjustments to the periodic theory can be undertaken and this approach leads to a theory identifying localized modes in media with weakly varying periodic behaviour. The two-scales approach outlined in this article provides a general methodology for treating doubly continuous periodic media, and can be extended to discrete periodic models consisting of point masses and springs. Such models are commonplace in solid state physics and they also exhibit band gap phenomena (Brillouin, 1953; Kittel, 1996). This, and other extensions of the theory are underway.

Acknowledgements

The authors thank NSERC (Canada) and the EPSRC (UK) for support through the Discovery Grant Scheme and grant EP/H021302 respectively. JK thanks the University of Alberta for its hospitality and support under the Visiting Scholar program. The authors gratefully acknowledge useful conversations with Sebastien Guenneau, Evgeniya Nolde and Valery Smyshlyaev.

References

Abramowitz, M. & Stegun, I. A. 1964 *Handbook of Mathematical Functions*. Washington: National Bureau of Standards.

Adams, S. D. M., Craster, R. V. & Guenneau, S. 2008 Bloch waves in periodic multi-layered waveguides. *Proc. R. Soc. Lond.* A **464**, 2669–2692.

Adams, S. D. M., Craster, R. V. & Guenneau, S. 2009 Negative bending mode curvature via Robin boundary conditions. *C. R. Physique* **10**, 437–446.

Andrianov, I. V., Bolshakov, V. I., Danishevs'kyy, V. V. & Weichert, D. 2008 Higher order asymptotic homogenization and wave propagation in periodic composite materials. *Proc. R. Soc. Lond.* A **464**, 1181–1201.

Arbogast, T., Douglas Jr., J. & Hornung, U. 1990 Derivation of the double porosity model of single phase flow via homogenization theory. *SIAM J. Math. Anal.* **21** (4), 823–836.

Babych, N. O., Kamotski, I. V. & Smyshlyaev, V. P. 2008 Homogenization of spectral problems in bounded domains with doubly high contrasts. *Networks and Heterogeneous Media* **3(3)**, 413–436.

Bakhvalov, N. & Panasenko, G. 1989 *Homogenization: Averaging Processes in Periodic Media*. Kluwer.

Bakhvalov, N. S. & Eglit, M. E. 2000 Effective dispersive equations for wave propagation in periodic media. *Doklady Mathematics* **370**, 1–4.

Bensoussan, A., Lions, J. & Papanicolaou, G. 1978 *Asymptotic analysis for periodic structures*. North-Holland, Amsterdam.

Berdichevski, V. L. 1983 *Variational principles of continuum mechanics*. Moscow: Nauka, in Russian.

Birman, M. S. 2004 On homogenization procedure for periodic operators near the edge of an internal gap. *St. Petersbg. Math. J.* **15** (4), 507–513.

Birman, M. S. & Suslina, T. A. 2006 Homogenization of a multidimensional periodic elliptic operator in a neighborhood of the edge of an internal gap. *J. Math. Sci.* **136** (2), 3682–3690.

Brillouin, L. 1953 *Wave propagation in periodic structures: electric filters and crystal lattices*, 2nd edn. Dover.

Cherednichenko, K. D., Smyshlyaev, V. P. & Zhikov, V. V. 2006 Non-local homogenized limits for composite media with highly anisotropic periodic fibres. *Proc. Roy. Soc. Edin.* **136**, 87–114.

Graff, K. F. 1975 *Wave motion in elastic solids*. Oxford University Press.

Gridin, D., Adamou, A. T. I. & Craster, R. V. 2004 Electronic eigenstates in quantum rings: Asymptotics and numerics. *Phys Rev B* **69**, 155317.

Gridin, D., Craster, R. V. & Adamou, A. T. I. 2005 Trapped modes in curved elastic plates. *Proc R Soc Lond A* **461**, 1181–1197.

Joannopoulos, J. D., Meade, R. D. & Winn, J. N. 1995 *Photonic Crystals, Molding the Flow of Light*. Princeton University Press, Princeton.

Kaplunov, J. D., Kossovich, L. Yu. & Nolde, E. V. 1998 *Dynamics of Thin Walled Elastic Bodies*. New York: Academic Press.

Kaplunov, J. D., Rogerson, G. A. & Tovstik, P. E. 2005 Localized vibration in elastic structures with slowly varying thickness. *Quart. J. Mech. Appl. Math.* **58**, 645–664.

Kittel, C. 1996 *Introduction to solid state physics*, 7th edn. John Wiley & Sons.

Kronig, R. L. & Penney, W. G. 1931 Quantum mechanics in crystals lattices. *Proc. R. Soc. Lond.* A **130**, 499–531.

Kushwaha, M. S., Halevi, P., Dobrzynski, L. & Djafari-Rouhani, B. 1993 Acoustic band structure of periodic elastic composites. *Phys. Rev. Lett.* **71**, 2022–2025.

Landau, L. D. & Lifshitz, E. M. 1970 *Theory of elasticity*, 2nd edn. Pergamon Press.

Le, K. C. 1999 *Vibrations of shells and rods*. Springer.

Love, A. E. H. 1944 *A treatise on the mathematical theory of elasticity*. Dover.

McIver, P. 2007 Approximations to wave propagation through doubly-periodic arrays of scatterers. *Waves in Random and Complex Media* **17**, 439–453.

McLachlan, N. W. 1964 *Theory and application of Mathieu functions*. Dover Publications.

Milton, G. W. 2002 *The Theory of Composites*. Cambridge: Cambridge University Press.

Moukhomodiarov, R. R., Pichugin, A. V. & Rogerson, G. A. 2010 The transition between Neumann and Dirichlet boundary conditions in isotropic elastic plates. *Math. Mech. Solids* Accepted for publication (available online doi:10.1177/1081286509103781).

Movchan, A. B., Movchan, N. V. & Poulton, C. G. 2002 *Asymptotic Models of Fields in Dilute and Densely Packed Composites*. ICP Press, London.

Parnell, W. J. & Abrahams, I. D. 2006 Dynamic homogenization in periodic fibre reinforced media. Quasi-static limit for SH waves. *Wave Motion* **43**, 474–498.

Poulton, C. G., McPhedran, R. C., Movchan, N. V. & Movchan, A. B. 2009 Convergence properties and flat bands in platonic crystal band structures using the multipole formulation. To appear in Waves in Random and Complex Media doi:10.1080/17455030903203140.

Poulton, C. G., McPhedran, R. C., Nicorovici, N. A., Botten, L. C. & Movchan, A. B. 2001 Asymptotics of photonic band structures for doubly-periodic arrays. In *IUTAM Symposium on Mechanical and Electromagnetic Waves in Structured Media* (ed. R. C. McPhedran, L. C. Botten & N. A. Nicorovici), pp. 227–238. New York: Kluwer.

Rayleigh, J. W. S. 1892 On the influence of obstacles arranged in rectangular order upon the properties of a medium. *Phil. Mag.* **34**, 481–502.

Sanchez-Palencia, E. 1980 *Non-homogeneous media and vibration theory*. Springer-Verlag.

Santosa, F. & Symes, W. W. 1991 A dispersive effective medium for wave propagation in periodic composites. *SIAM J. Appl. Math.* **51(4)**, 984–1005.

Smith, D. R., Pendry, J. B. & Wiltshire, M. C. K. 2004 Metamaterials and negative refractive index. *Science* **305**, 788–792.

Smyshlyaev, V. P. 2009 Propagation and localization of elastic waves in highly anisotropic periodic composites via two-scale homogenization. *Mech. Materials* **41**, 434–447.

Smyshlyaev, V. P. & Cherednichenko, K. D. 2000 On rigorous derivation of strain gradient effects in the overall behaviour of periodic heterogeneous media. *J. Mech. Phys. Solids* **48**, 1325–1357.

Weideman, J. A. C. & Reddy, S. C. 2000 A MATLAB differentiation matrix suite. *ACM Trans. Math. Software* **26**, 465–519.

Zolla, F., Renversez, G., Nicolet, A., Kuhlmey, B., Guenneau, S. & Felbacq, D. 2005 *Foundations of photonic crystal fibres*. Imperial College Press, London.